HHS Public Access

Author manuscript

*Curr Top Med Chem*. Author manuscript; available in PMC 2021 January 01.

Published in final edited form as:

*Curr Top Med Chem*. 2020 ; 20(5): 367–376. doi:10.2174/1568026620666200101095641.

# Mathematical Modeling to Address Challenges in Pancreatic Cancer

**Prashant Dogra**[1], **Javier Ruiz Ramírez**[1], **María J. Peláez**[1,2], **Zhihui Wang**[1], **Vittorio Cristini**[1], **Gulshan Parasher**[3], **Manmeet Rawat**[3,*]

[1]Mathematics in Medicine Program, Houston Methodist Research Institute, Houston, TX 77030, USA.

[2]Applied Physics Graduate Program, Rice University, Houston, TX 77005, USA.

[3]Department of Internal Medicine, University of New Mexico School of Medicine, Albuquerque, NM 87131, USA.

## Abstract

Pancreatic ductal adenocarcinoma (PDAC) is regarded as one of the most lethal cancer types for its challenges associated with early diagnosis and resistance to standard chemotherapeutic agents, thereby leading to a poor five-year survival rate. The complexity of the disease calls for a multidisciplinary approach to better manage the disease and improve the status quo in PDAC diagnosis, prognosis, and treatment. To this end, the application of quantitative tools can help improve the understanding of disease mechanisms, develop biomarkers for early diagnosis, and design patient-specific treatment strategies to improve therapeutic outcomes. However, such approaches have only been minimally applied towards the investigation of PDAC, and we review the current status of mathematical modeling works in this field.

### Keywords

mathematical modeling; numerical simulation; desmoplasia; pancreatic ductal adenocarcinoma

## Introduction

Approximately 420,000 new cases of pancreatic cancer will have been diagnosed globally by 2020, of which ~410,000 patients are estimated to die [1]. Of these cases, 93% will be pancreatic ductal adenocarcinomas (PDAC) occurring in the exocrine part of the pancreas, and the remaining 7% will be pancreatic neuroendocrine tumors developing in the endocrine portion of the pancreas [2]. PDAC has very poor prognosis with a 5-year survival rate of ~5%, and <11-months of median survival. Thus, PDAC ranks as the third most lethal form of cancer after lung and colon [2]. The incidence of PDAC is expected to increase, with

*Correspondence should be sent to: **Manmeet Rawat, Ph.D,** Department of Internal Medicine, University of New Mexico School of Medicine, 1 University of New Mexico, MSC10-5550, Albuquerque, NM 87131-0001, USA, manmeetrawat@gmail.com, mrawat@salud.unm.edu.

Conflicts of interest

The authors declare no conflicts of interest.

projections of more than two-fold rise in the number of new diagnoses and PDAC-related deaths within the next ten years [3]. In addition to demographic factors like age, gender, and ethnicity, other risk factors associated with PDAC include smoking, chronic diabetes mellitus, chronic pancreatitis, obesity or sedentary lifestyle, non-O blood group, and genetic susceptibility [4, 5]. Progression from healthy mucosa to invasive malignant PDAC occurs via a series of step-wise mutations that lead to the development of pre-cancerous precursor lesions namely, pancreatic intraepithelial neoplasm (PanIN), intraductal papillary mucinous neoplasm (IPMN), and mucinous cystic neoplasm (MCN), each bearing characteristic molecular, pathological, and clinical features [6]. The pathophysiological hallmarks of PDAC include nearly 100% KRAS mutation frequency [7]; strong desmoplastic reaction that leads to a dense extracellular matrix, hypovascularity, hypoxia, reprogrammed cell metabolism, evasion of immunity [8]; and a heightened tendency for local invasion and distant metastasis [9].

PDAC poses significant challenge in early diagnosis and is generally diagnosed in patients above 40 years of age, with the median age of diagnosis being 71 years, and the majority of cases presenting with a locally advanced or metastatic disease with nodal involvement [4, 5]. Sensitive and accurate serum biomarkers for early detection of PDAC are a work in progress. Carbohydrate antigen 19–9 (CA 19–9) and carcinoembryonic antigen (CEA) are the only two clinically used serum biomarkers for PDAC, but they suffer from low sensitivity and specificity [10]. Other biomarkers like circulating tumor cells or circulating tumor DNA suffer from similar issues of limited sensitivity or specificity [10]. MicroRNAs isolated from pancreatic tumor tissue, blood samples, pancreatic juice, stool, urine, and saliva are also being investigated for their diagnostic value [11]. Imaging techniques, such as computed tomography (CT scan), endoscopic ultrasound (EUS), and magnetic resonance imaging (MRI) are commonly used to confirm the diagnosis and to help assess whether the tumor is surgically resectable. Due to poor diagnosis and early metastasis of the disease, only few patients are eligible for curative-intent surgery, and thus systemic chemotherapy is the mainstay of treatment for patients diagnosed with PDAC, with the chemotherapeutics of choice being gemcitabine, 5-fluorouracil, capecitabine, and folfirinox [11–13]. With improvements in understanding of the *in vivo* behavior of nanomaterials [14–16], the development of novel nanoparticle-based therapies for cancer diagnosis and treatment has seen a surge in the past decade [17, 18]. This has also led to the development of nanomaterials for improved delivery of drugs in PDAC [19–21]. However, the clinical translation of such novel drug delivery platforms has been limited primarily due to preferential accumulation of nanomaterials in the mononuclear phagocytic system and heterogenous tumor penetration [22, 23]. Checkpoint inhibitor monoclonal antibodies in combination with other agents are also being investigated to overcome the immunosuppressive microenvironment of PDAC and recruit effector T cells for effective treatment [24].

Over the last two decades considerable progress has been achieved in basic or translational research involving PDAC. However, the application of mathematical and computational tools to support explorations in PDAC biology, diagnosis, prognosis, and treatment has lagged behind, and this becomes even more evident when compared to the progress made in quantitative investigations of other cancer types (Figure 1) [25–41]. This gap highlights the

need for the development and application of novel quantitative tools to improve the understanding of PDAC progression and support clinical care. Here, we review mathematical modeling efforts undertaken to understand PDAC progression, and explore their applications in PDAC diagnosis, prognosis, drug delivery, and precision medicine.

## Mathematical models of PDAC progression: Applications in treatment

The discrepancy between the highly successful *in vitro* efficacy of a therapeutic agent and its suboptimal performance *in vivo* can be attributed to tumor microenvironment variables that can radically influence drug delivery and cytotoxic potential of the drug, and simultaneously alter the aggressiveness of the targeted cells [42–44]. To this end, Lee *et al.* [45] combined *in vitro* cytotoxicity data with nutrient and oxygen concentration gradient dependent cell proliferation and death parameters to inform a nonlinear mathematical model of PDAC progression, which is an adaptation of a model developed by Cristini *et al.* [46–48]. The model assumes a quasi-steady state diffusion-reaction equation to describe the concentration of cell substrates (nutrients) throughout the tumor domain:

$$\nabla^2\sigma - R = 0 \tag{1}$$

where $\sigma$ is the concentration of substrate and $R$ denotes the substrate addition rate, which incorporates i) the transport of material from the vasculature and ii) the loss of material due to the intrinsic consumption by tumor cells. The model also assumes that the cells move with velocity $\boldsymbol{u}$ due to intratumoral pressure gradients. The governing equation for the velocity follows the Darcy flow expression:

$$\boldsymbol{u} = -\mu\nabla P \tag{2}$$

where $\mu$ denotes the cell mobility, and $P$ is the intratumoral pressure.

Lastly, the equation that couples the concentration with the pressure is a characterization of the sinks and sources of cells in the domain. This is accomplished by means of the divergence operator applied to the velocity. Namely, $\nabla \cdot \boldsymbol{u} = \lambda_p$, where $\lambda_p$ depends on the concentration of cells, their mitotic rate $b$ and their apoptotic rate $\lambda_A$. Explicitly, $\lambda_p = b\sigma - \lambda_A$.

The model was informed by *in vitro* experiments on pancreatic cancer cell lines for cellular proliferation and apoptosis rates and used to simulate tumor growth and test the efficacy of gemcitabine. As shown in Figure 2, for the concentrations of the chemotherapeutic agent under consideration, the growth of the tumor always remained positive, which is consistent with *in vivo* observations on an orthotopic tumor model with the same cell line. This model provides a tool to simulate tumor growth under variable scenarios and thus predict therapeutic efficacy.

In the aforementioned model, the governing equations are deterministic and consider a localized tumor that grows in time but that does not invade proximal and distal tissues. However, in reality, several of the mechanisms that drive the evolution of cancer are stochastic in nature. Furthermore, one of the hallmarks of PDAC is metastasis. Hence, a

model capable of incorporating these two aspects could be especially useful in predicting survival rates for patients. Moreover, with the appropriate parameters, it could be used to quantify the population of metastatic cells as a function of time, giving reasonable estimates for the progression of the disease. To this end, Haeno *et al.* [49] model cancer metastasis as a random process and assume an initial exponential growth using a rule-based modeling approach. To generate and later test their model, they use data from two clinical databases. The key players in the model are cancer cells classified into three categories, type 0, type 1, and type 2. Type 0 is characterized by non-metastatic cells residing in the primary tumor that possess a proliferation rate $r$ and a death rate $d$. Type 1 cells are metastatic and originate from type 0 cells possibly through epigenetic mutations at a rate $u$ per cell division. Similar to type 0 cells, type 1 cells continue to reside within the primary tumor and migrate to adjacent regions at a rate $q$ to finally become type 2 cells. The proliferation and death rates for the cell type $k$ for $k = 1,2$, is given by the constants $a_k$ and $b_k$, respectively.

The system initiates with $M_1$ tumor cells, cell fitness is assessed, and the aforementioned transition rules are applied to 4 different scenarios: (i) no treatment, (ii) the patient has surgery and a fraction of the primary tumor is removed, (iii) chemoradiation or chemotherapy is administered diminishing the proliferation rate of all cell populations by a certain factor, and (iv) the patient undergoes both surgery and chemoradiation/chemotherapy. The parameters $u$ (conversion into type 1) and $q$ (migration) are determined through the available clinical data of tumor metastasis and computed, by means of probability generating functions [50]. The model was used to test the effect of variable treatment regimens on patient survival. Finally, we mention that a generalization to Haeno *et al.* [49] can be found in Yamamoto *et al.* [51], where the authors include the effects of metastasis suppressor genes and epithelial mesenchymal transition. Other avenues that also follow a stochastic approach based on the methods of Haeno *et al.* [49] involve the analysis of the effects of the genes KRAS, CDKN2A, TP53, and SMAD4 in determining the likelihood of the cancer becoming metastatic [52], and the investigation of optimal strategies in administering therapies consisting of the drugs Folfirinox, gemcitabine, and the combination of gemcitabine with nab-paclitaxel [53]. In all instances, the numerical results generated by the simulations correlated with the available clinical data.

Further, to elucidate the cause of drug resistance in PDAC, Yachida *et al.* [54] sequenced seven PDAC metastases and compared their clonal profile against primary and metastatic neoplasms, to test two hypotheses: i) cancer is detected too late, at a point where the damage is irreversible, and ii) cells become metastatic and migrate at a fairly early stage. To investigate this, they developed a mathematical model based on a Poisson process [55]. With this technique the authors concluded that on average 10 years elapse from the origin of the non-metastatic founder cell to the point where its lineage begins to exhibit the first traces of a metastatic mutation. Furthermore, they discovered that 5 additional years are necessary for the cells to fully develop their metastatic potential. From this point onwards the spread of the disease is extensive and the patients live on average 2 years. Thus, one can identify three relevant periods of time in the model. T1, the time between the origin of the founder cell and the first mutation, T2, the time after T1 acquires a completely functional metastatic potential, and T3, the remaining lifespan of the patient after T2.

We remark that a refinement of Yachida *et al.* [54] can be found in Makohon-Moore *et al.* [56], where the authors provide a more detailed description of the type of lesions under consideration. For instance, they make the distinction between PDAC, low-grade pancreatic intraepithelial neoplastic lesions (LG-PanIN) that possess a medium level of cytological abnormalities, and high-grade PanIN (HG-PanIN) with extensive cytological mutations that are hypothesized to enable the cancer to penetrate surrounding tissue. Furthermore, the proposed model considers three scenarios based on the number of somatic mutations that are shared between the various types of lesions. These mutations are in turn divided into two driver genes D1 and D2, whose simultaneous presence is necessary to result in an activated metastatic potential. The first scenario assumes no commonalities between the mutations and hence D1 is unique to PDAC and D2 is unique to PanIN. In the second case, an ancestral cell leads to the formation of PanIN and PDAC lineages by means of a founder cell, where both the founder cell and PanIN lack the metastatic potential. Hence, the founder cell possesses the first driver mutation D1 and PDAC the second D2, becoming fully metastatic. Finally, in the third scenario, the ancestral cell produces a metastatic founder cell having both driver mutations D1 and D2.

Pancreatic stellate cells (PSCs) are particularly relevant in processes that lead to pancreatic fibrosis, which is a hallmark of PDAC. Transcription factor STAT1 (signal transducer and activator of transcription 1) mediated interferon-$\gamma$ (IFN-$\gamma$) signaling in PSCs is believed to reduce tumor progression by either inhibiting fibrogenesis, or by having a direct effect on the proliferation of tumor cells. To answer their question, Lange *et al.* [57] proposed a signaling pathway and developed a systems model comprising a system of ordinary differential equations (ODEs) that were solved numerically. Interestingly, their model incorporates delay terms, resulting in a system of delayed differential equations. Combining clinical data and their mathematical model, the authors concluded that the effectiveness of IFN-$\gamma$ was independent of the presence of PSCs. Moreover, they observed that when PSCs are present the key mechanism is through fibrogenesis inhibition and that in their absence it is probably due to a combination of inhibitory effects on cells local to the microenvironment and the direct action on tumor cells. It is noteworthy to mention that in a follow-up study, Lange *et al.* [58] were able to generate numerical results consistent with observed experimental clinical data related to the selective tyrosine-kinase inhibitor drug erlotinib. Their findings provided supporting evidence to the proposed mechanisms of action and explain the effectiveness of erlotinib.

A detailed systems biology model of PDAC progression that incorporated cancer-stroma-immune interactions was developed by Louzoun *et al.* [59]. The model consisted of a system of 11 ODEs representing the following variables: pancreatic cancer cells (PCCs), PSCs, pro-inflammatory macrophages (M1), anti-inflammatory macrophages (M2 & MDSCs), cytotoxic T cells (CTL), and primary cytokines (TGFβ, IL6, MCSF, GMCSF, IL10 and IL12). In order to simplify the model, they used quasi-steady-state approximations for cytokine concentrations and ended up with four ODEs where the species of interest were: the density of PCCs, the density of PSCs, the density of CTL, and a new variable representing the ratio of M1/(M1+M2) macrophages. The model was validated with data from published literature and was used to investigate the relationship between drug efficacy and immune response. It was observed that immunotherapy is only effective when the killing

rate of cancer cells by T cells ($\lambda_c$) and the parameters describing the effect of PCCs and PSCs ($\gamma_c, \gamma_p$, respectively) on polarization of the macrophages fall within a specific range, suggesting that the immune system has a certain window of opportunity to efficiently suppress cancer under treatment. When $\gamma_c = 0$ and $\gamma_p = 0$, the steady state of tumor size $C$ slowly decreases as $\lambda_c$ increases, however if the values are non-zero, there is a faster decline in $C$. Further, it was seen that at $\lambda_c$=5e-8, $C$ remains high regardless of the values of $\gamma_c$ and $\gamma_p$, but if $\lambda_c$ = 5e-7, $C$ decreases significantly at low values of $\gamma_c$ and $\gamma_p$.

To describe pancreatic cancer progression under therapy, Chen *et al.* [60] used a cell-based mathematical modeling approach (Figure 3). The model is based on the following key simplifications: considers only three cell phenotypes (epithelial cells, cancer cells, and T-lymphocytes), considers two possible states for each cell (dead or viable), and assumes a uniform collagen density for the desmoplastic stroma. The migration of epithelial and cancer cells was modeled using the strain energy density, the total repulsive force, and random walks. T-lymphocytes migration modeling took into account chemotaxis, mechanical repulsion, random walk, and small range impingement. The probability of cell division, mutation, and death was simulated with stochastic processes. A two-dimensional orientation is created to simulate the changes in migration of the T-lymphocytes due to the orientation of the desmoplastic ECM. Treatment injection is modeled as a source point with a diffusive behavior afterwards. Monte Carlo simulations were used to investigate the propagation of uncertainties in the parameters and after each simulation is completed, the final fraction of cancer cells is calculated as an evaluation criterion for cancer development. The authors used the model to compare the effectiveness of PEGPH20 and gemcitabine therapy at different stages of diagnosis. It was observed that the final fraction of cancer cells is dependent on the fraction of cancer cells on which the treatments is initiated. This model can be used for testing treatment efficacy and could be used to design drug dosage regimen.

The kinetic model constructed by Roy *et al.* [61] consists of a system of 47 ODEs that intended to describe the metabolic network dynamics involved in glycolysis, glutaminolysis, tricarboxylic acid cycle (TCA), and the pentose phosphate pathway (PPP) in PDAC. It is based on *a* priori knowledge of the 46 metabolites involved in the different pathways and the 53 reactions and interactions between them. Each metabolite concentration change rate is represented by one ODE and the final ODE describes the time evolution of the number of cancer cells. Each metabolite's initial concentration had the possibility to vary within a specific range; Latin Hypercube Sampling was applied to efficiently explore the entire spectrum of possibilities. In order to obtain the parameters for the model, only the reaction velocities and the growth parameters were fitted into the training data, and the rest of them used literature values. To validate the model, the authors used available experimental measurements for cell proliferation under conditions of nutrient deprivation. To test the robustness of the model they performed Monte Carlo analysis on the increase in number of cancer cells for varying metabolite initial conditions. The result of these simulations indicate that cell proliferation is sensitive to the initial metabolite concentrations. This model predicts a nonlinear influence of glucose and glutamine availability on cell proliferation and a stronger dependency of the number of pancreatic cells with glutamine availability, as compared to glucose. By predicting the dynamic reaction fluxes under varying conditions, the model is also able to provide insight into the metabolic phenotype of the pancreatic

cancer cells. Additionally, the model has the capability of predicting system-level response to various metabolic perturbations and novel strategies to reduce cell proliferation. Using this model, the authors were able to show the importance of targeting the PPP, TCA cycle, and mitochondrial-cytoplasmic shuttle reactions for regulating tumor metabolism.

Using *a priori* knowledge of signaling pathways in pancreatic cancer, Gong *et al.* [62] developed a Boolean network model to study the interplay between tumor growth, cell cycle arrest, and apoptosis. The major signaling pathways included were: the Hedgehog, WNT, KRAS, RB-E2F, NFκB, p53, TGFβ, and apoptosis pathways. The input signals for the model represent different growth factors; the output signals are apoptosis, proliferation, and cell arrest. Each node in the model represents a protein or lipid in the signaling pathway, and it has two states: ON (1) or OFF (0). The time evolution of each node state is described by a Boolean transfer function that depends on the neighbor's node state. The total Boolean network consisted of 61 nodes, which included 7 input nodes and 3 output nodes. Symbolic Model Checking was used to verify that the model satisfies temporal logic properties related to cell fate, cell cycle, and oscillations. In order to use it, the model's intended behaviors were expressed as Computation Tree Logic formulas. Some results that the model provides are: (i) inhibition of apoptosis and cell cycle arrest are not unavoidable and permanent, (ii) apoptosis can be activated even when p53 is not, (iii) an initial overexpression of TGFβ or PIP3 always leads to oscillations in the expression level of NFκB's. The model results present new interesting properties for future testing.

## Mathematical models for PDAC diagnosis and prognosis

### Imaging-based diagnosis and prognosis

The metastatic potential of PDAC has been found to be controlled by the stroma around the tumor, hence certain characteristics of the stroma may serve as measurable biomarkers to assess PDAC aggresiveness. To investigate this, Koay *et al.* used quantitative computed tomography (CT) imaging on preoperative tumors to measure the "delta" value at the tumor-normal tissue interface [63]. The "delta" value is defined as the difference between the mean Hounsfield unit value of the tumor contour and the normal tissue contour at the interface. The "delta" measurement was used for a binary classification of patients into high-delta and low-delta that correlated with more aggressive and less aggressive disease, respectively. High-delta patients also demonstrated poorer response to therapy than low-delta patients. To investigate the biophysical mechanisms leading to the morphological differences in PDAC tumors, they developed a mathematical model of macroscopic tumor progression that accounts for cell proliferation and cell migration. The model is based on a multicomponent mixture modeling framework that accounts for the tumor and healthy tissue comprising of a mixture of viable and dead cells with volume fractions $\phi_V$ and $\phi_D$, respectively. The mass balance equation describing the temporal evolution of $\phi_V$ or $\phi_D$ is:

$$\frac{\partial \phi_i}{\partial t} + \nabla \bullet (u_i \phi_i) = -\nabla \bullet J_i + S_i, \qquad i = V, D \tag{3}$$

where, $u_i$ is the velocity, $J_i$ is a flux, and $S_i$ is a source term accounting for cell proliferation and death. The model is used to numerically simulate tumors with cell proliferation rate

($\Lambda_P$) lower than cell migration rate ($\Lambda_M$), and tumors with the opposite behavior. The stability parameter $\Lambda = \Lambda_P/\Lambda_M$ characterizes the stability of the tumor-host tissue interface, and as shown in Figure 4, low $\Lambda$ values show tumor intermingling with stroma, which is representative of low-mode instability that manifests as finger-like projections, and high $\Lambda$ produces simulations of tumors with distinct tumor-stroma interface. The simulation results were analogous to macroscopic features observed in patient CT scans (Figure 4a,c). Thus, using the mathematical model they explain the observed phenomena of high- and low-delta tumors, and provide a tool based on standard CT scans that can be used pre-treatment to predict disease prognosis and thus tailor patient-specific treatments.

To improve the diagnosis of PDAC and be able to accurately differentiate between cancerous and non-cancerous pancreatic lesions, Bali *et al.* [64] used quantitative parameters obtained from mathematical modeling of dynamic contrast enhanced magnetic resonance imaging (DCE MRI) data to correlate with fibrosis content and microvascular density (MVD) in the lesions. They used one-compartment and two-compartment pharmacokinetic models to fit to the contrast enhancement kinetics data obtained from DCE MRI, in order to estimate mechanistic parameters that characterize the transport properties of the contrast agent in the lesions. Contrast enhancement kinetics is modeled using the following equations:

### One compartment model:

$$C_T(t) = K^{trans} \int_0^t C_{art}(t') e^{-\frac{K^{trans}(t-t')}{f}} dt' \quad (4)$$

where, $C_T$ and $C_{art}$ represent the concentration of contrast agent in tissue interstitium and abdominal aorta, respectively; $K^{trans}$ is the mass transfer rate constant representing the transvascular transfer of contrast agent; and $f$ is the volume fraction of tissue available to the contrast agent (includes, plasma and extravascular extracellular space).

### Two compartment model:

$$C_T(t) = K^{trans} \int_0^t C_{art}(t') e^{-\frac{K^{trans}(t-t')}{v_i}} dt' + v_p C_{art}\left(t\right) \quad (5)$$

where, $v_p$ and $v_i$ represent the tissue volume fraction occupied by plasma and extravascular extracellular space, respectively. The two-compartment model is permeability-limited, while the one compartment model is perfusion-limited. As a result, the $K^{trans}$ parameter in the one compartment model is a measure of tissue perfusion, rather than of tissue permeability, and fits the DCE MRI data for hypovascular lesions that have low tissue perfusion better than the two-compartment model. Overall, the $K^{trans}$ values were lower for malignant tumors than for benign lesions and healthy tissue. Also, the two-compartment model revealed smaller values of $v_p$ for hypovascular tumors and also for benign lesions and healthy pancreatic tissues. However, in hypervascular tumors the two-compartment model provided better fits and larger values for the $v_p$ parameter. Further, the estimates of model parameters showed significant correlation with histopathological measures of fibrosis and MVD. $K^{trans}$ estimates from the two models were negatively correlated with fibrosis content in the lesion,

whereas $f$ and $v_i$ showed a positive correlation with fibrosis content and MVD. This study thus demonstrates the application of DCE MRI and pharmacokinetic modeling as a prognostic and diagnostic tool for pancreatic lesions.

A similar approach was employed by Liu *et al.* where they used two-compartment and three-compartment pharmacokinetic models to estimate transport parameters from DCE MRI data of PDAC patients to test the correlation with tumor fibrosis and vascularization [65]. The analysis revealed significant correlations between the pharmacokinetic model parameters and tumor characteristics like fibrosis and vascular density, further supporting the application of integrated DCE MRI imaging with mathematical modeling for predictive applications in the clinic.

### Blood biomarker-based diagnosis

In order to improve early diagnosis of PDAC, a mathematical model was developed by Root *et al.* to investigate the feasibility of application of blood-based biomarkers in PDAC detection [66]. The model consists of a mass balance-based ODE that defines the blood concentration kinetics of the biomarker by taking into account biomarker secretion into blood from normal and cancerous cells, and its elimination (clearance) from the blood (Equation 6).

$$\frac{dB}{dt} = f s_c V_c(t) + f s_n V_n - k B\left(t\right) \tag{6}$$

where, $B$ represents blood biomarker concentration; $f$ represents the fraction of biomarker entering the blood from tumor or healthy tissue interstitium; $s_c$ and $s_n$ are the rates of shedding or secretion of biomarker from the cancerous and normal cells, respectively; $k$ is the rate of excretion of the biomarker from blood; $V_c$ and $V_n$ represent the volume of tumor and healthy tissue, respectively. $V_n$ is assumed to be constant and $V_c$ grows exponentially over time as defined by the tumor growth equation: $V_c(t) = V_0 e^{gt}$. $V_0$ is the volume of primary tumor at diagnosis, and $g$ is the tumor growth rate constant.

Model simulations reveal that PDAC detection through a blood-based biomarker is feasible and can help with detection almost a year and a half before the lower limit for detection through imaging is reached, provided the biomarker production rate is moderately high.

## Mathematical models of drug delivery in PDAC

The traditionally accepted predictor of therapeutic efficacy, i.e. plasma drug concentration kinetics may not reflect the drug concentration kinetics in the vicinity of cancerous cells due to the barriers to drug diffusion imposed by the dense extracellular matrix of PDAC. Thus, the tumor microenvironment of PDAC plays a crucial role in the transport of drug molecules from the tumor microvasculature to the cancerous cells. Further, due to patient- or tumor-specific variability, a greater difference in the tumor site drug concentration may exist across patients, thereby leading to differential therapy response to gold-standard treatment regimens in the patient population. To investigate the role of mass transport properties of the PDAC microenvironment in inducing therapeutic resistance to gemcitabine, Koay et al. conducted a clinical trial on patients with resectable primary PDAC tumors that were administered

intraoperative gemcitabine infusion during curative-intent surgery [67]. Using integrated CT imaging and mathematical modeling, they estimated transport parameters of the tissue and assessed their correlation with incorporation of gemcitabine in the cellular DNA. Also, they investigated the correlation of transport properties with response to neoadjuvant therapy (Figure 5). The mathematical model consists of an ODE that models the density kinetics of the contrast agent in the tissue of interest:

$$\frac{dY}{dt} = R\left(Y_{\max}^{V} e^{-R_c t} - Y\right) \tag{7}$$

where, $Y$ is the density of contrast in the tissue at time $t$, $Y_{\max}^{V}$ is the imposed density of contrast in the vasculature, $R$ is the transvascular mass transfer rate constant, and $R_c$ is the rate of excretion of the contrast agent from blood. Following fitting of the model to CT data from individual patient scans, the estimated transport parameter (normalized area under the curve (AUC)) correlated inversely with gemcitabine incorporation into tumor DNA and with response to therapy, indicating that better transport improves drug delivery and thus treatment outcome. The study provides a clinical tool that can be used to assess the transport properties of PDAC and other solid tumors and design treatment regimens accordingly. A follow up study on the same patients was then conducted to understand intratumoral heterogeneity in gemcitabine transport, which revealed significant differences in drug transport within a tumor and across the patient population as determined by the drug transport model parameter estimates [68].

## Conclusions

The challenges associated with early diagnosis and drug resistance in PDAC make it one of the most lethal cancer types. For improved pathophysiological understanding of the disease, development of novel biomarkers for early diagnosis, investigation of the effects of inter-individual and intra-tumoral-heterogeneity, a multidisciplinary approach involving basic research, imaging, and mathematical modeling holds the key to bring a significant change in the state of affairs. In this review, we highlight such interdisciplinary studies that have performed to model PDAC disease progression for testing therapy efficacy, develop biomarkers for early diagnosis, and investigate drug delivery challenges due to pathological conditions in the tumor It is essential to invest more efforts in the direction of personalized treatment through the application of quantitative tools to overcome the status quo in the clinical management of PDAC.

## Acknowledgements

This research has been supported in part by the National Science Foundation Grant DMS-1930583 (ZW, VC), the National Institutes of Health (NIH) Grants 1U01CA196403 (ZW, VC), 1U01CA213759 (ZW, VC), 1R01CA226537 (ZW, VC), 1R01CA222007 (ZW, VC), and U54CA210181 (ZW, VC).

## References

[1]. Ferlay J; Soerjomataram I; Dikshit R; Eser S; Mathers C; Rebelo M; Parkin DM; Forman D; Bray F, Cancer incidence and mortality worldwide: sources, methods and major patterns in

GLOBOCAN 2012. International journal of cancer, 2015, 136, (5), E359–E386. [PubMed: 25220842]

[2]. Siegel RL; Miller KD; Jemal A, Cancer statistics, 2019. CA: a cancer journal for clinicians, 2019, 69, (1), 7–34. [PubMed: 30620402]

[3]. Orth M; Metzger P; Gerum S; Mayerle J; Schneider G; Belka C; Schnurr M; Lauber K, Pancreatic ductal adenocarcinoma: biological hallmarks, current status, and future perspectives of combined modality treatment approaches. Radiation Oncology, 2019, 14, (1), 1–20. [PubMed: 30621744]

[4]. Ryan DP; Hong TS; Bardeesy N, Pancreatic adenocarcinoma. New England Journal of Medicine, 2014, 371, (11), 1039–1049.

[5]. McGuigan A; Kelly P; Turkington RC; Jones C; Coleman HG; McCain RS, Pancreatic cancer: A review of clinical diagnosis, epidemiology, treatment and outcomes. World journal of gastroenterology, 2018, 24, (43), 4846. [PubMed: 30487695]

[6]. Riva G; Pea A; Pilati C; Fiadone G; Lawlor RT; Scarpa A; Luchini C, Histo-molecular oncogenesis of pancreatic cancer: From precancerous lesions to invasive ductal adenocarcinoma. World journal of gastrointestinal oncology, 2018, 10, (10), 317. [PubMed: 30364837]

[7]. Waters AM; Der CJ, KRAS: the critical driver and therapeutic target for pancreatic cancer. Cold Spring Harbor perspectives in medicine, 2018, 8, (9), a031435. [PubMed: 29229669]

[8]. Cannon A; Thompson C; Hall BR; Jain M; Kumar S; Batra SK, Desmoplasia in pancreatic ductal adenocarcinoma: insight into pathological function and therapeutic potential. Genes & cancer, 2018, 9, (3–4), 78. [PubMed: 30108679]

[9]. Le Large T; Bijlsma M; Kazemier G; van Laarhoven H; Giovannetti E; Jimenez C In Seminars in cancer biology; Elsevier, 2017; Vol. 44, pp 153–169. [PubMed: 28366542]

[10]. E Poruk K; Z Gay D; Brown K; D Mulvihill J; M Boucher K; L Scaife C; A Firpo M; J Mulvihill S, The clinical utility of CA 19–9 in pancreatic adenocarcinoma: diagnostic and prognostic updates. Current molecular medicine, 2013, 13, (3), 340–351. [PubMed: 23331006]

[11]. Rawat M; Kadian K; Gupta Y; Kumar A; Chain PS; Kovbasnjuk O; Kumar S; Parasher G, MicroRNA in Pancreatic Cancer: From Biology to Therapeutic Potential. Genes, 2019, 10, (10), 752.

[12]. Moore MJ; Goldstein D; Hamm J; Figer A; Hecht JR; Gallinger S; Au HJ; Murawa P; Walde D; Wolff RA, Erlotinib plus gemcitabine compared with gemcitabine alone in patients with advanced pancreatic cancer: a phase III trial of the National Cancer Institute of Canada Clinical Trials Group. Journal of clinical oncology, 2007, 25, (15), 1960–1966. [PubMed: 17452677]

[13]. Conroy T; Desseigne F; Ychou M; Ducreux M; Bouche O; Guimbaud R; Becouarn Y; Montoto-Grillot C; Gourgou-Bourgade S; Adenis A, Randomized phase III trial comparing FOLFIRINOX (F: 5FU/leucovorin [LV], irinotecan [I], and oxaliplatin [O]) versus gemcitabine (G) as first-line treatment for metastatic pancreatic adenocarcinoma (MPA): preplanned interim analysis results of the PRODIGE 4/ACCORD 11 trial. Journal of Clinical Oncology, 2010, 28, (15_suppl), 4010–4010.

[14]. Dogra P; Adolphi NL; Wang Z; Lin Y-S; Butler KS; Durfee PN; Croissant JG; Noureddine A; Coker EN; Bearer EL; Cristini V; Brinker CJ, Establishing the effects of mesoporous silica nanoparticle properties on in vivo disposition using imaging-based pharmacokinetics. Nature Communications, 2018, 9, (1), 4551.

[15]. Tsoi KM; MacParland SA; Ma X-Z; Spetzler VN; Echeverri J; Ouyang B; Fadel SM; Sykes EA; Goldaracena N; Kaths JM, Mechanism of hard-nanomaterial clearance by the liver. Nature Materials, 2016.

[16]. Brocato TA; Coker EN; Durfee PN; Lin Y-S; Townson J; Wyckoff EF; Cristini V; Brinker CJ; Wang Z, Understanding the Connection between Nanoparticle Uptake and Cancer Treatment Efficacy using Mathematical Modeling. Scientific reports, 2018, 8, (1), 7538. [PubMed: 29795392]

[17]. Goel S; Ferreira CA; Dogra P; Yu B; Kutyreff CJ; Siamof CM; Engle JW; Barnhart TE; Cristini V; Wang Z; Cai W, Size-Optimized Ultrasmall Porous Silica Nanoparticles Depict Vasculature-Based Differential Targeting in Triple Negative Breast Cancer. Small, 2019, e1903747. [PubMed: 31565854]

[18]. Hosoya H; Dobroff AS; Driessen WHP; Cristini V; Brinker LM; Staquicini FI; Cardó-Vila M; D'Angelo S; Ferrara F; Proneth B; Lin Y-S; Dunphy DR; Dogra P; Melancon MP; Stafford RJ; Miyazono K; Gelovani JG; Kataoka K; Brinker CJ; Sidman RL; Arap W; Pasqualini R, Integrated nanotechnology platform for tumor-targeted multimodal imaging and therapeutic cargo release. Proceedings of the National Academy of Sciences, 2016, 113, (7), 1877–1882.

[19]. Liu X; Situ A; Kang Y; Villabroza KR; Liao Y; Chang CH; Donahue T; Nel AE; Meng H, Irinotecan delivery by lipid-coated mesoporous silica nanoparticles shows improved efficacy and safety over liposomes for pancreatic cancer. ACS nano, 2016, 10, (2), 2702–2715. [PubMed: 26835979]

[20]. Meng H; Wang M; Liu H; Liu X; Situ A; Wu B; Ji Z; Chang CH; Nel AE, Use of a lipid-coated mesoporous silica nanoparticle platform for synergistic gemcitabine and paclitaxel delivery to human pancreatic cancer in mice. ACS nano, 2015, 9, (4), 3540–3557. [PubMed: 25776964]

[21]. Meng H; Zhao Y; Dong J; Xue M; Lin Y-S; Ji Z; Mai WX; Zhang H; Chang CH; Brinker CJ, Two-wave nanotherapy to target the stroma and optimize gemcitabine delivery to a human pancreatic cancer model in mice. ACS nano, 2013, 7, (11), 10048–10065. [PubMed: 24143858]

[22]. Wilhelm S; Tavares AJ; Dai Q; Ohta S; Audet J; Dvorak HF; Chan WCW, Analysis of nanoparticle delivery to tumours. Nature Reviews Materials, 2016, 1, 16014.

[23]. Dogra P; Butner JD; Chuang Y.-l.; Caserta S; Goel S; Brinker CJ; Cristini V; Wang Z, Mathematical modeling in cancer nanomedicine: a review. Biomedical Microdevices, 2019, 21, (2), 40. [PubMed: 30949850]

[24]. Hilmi M; Bartholin L; Neuzillet C, Immune therapies in pancreatic ductal adenocarcinoma: Where are we now? World journal of gastroenterology, 2018, 24, (20), 2137. [PubMed: 29853732]

[25]. Chauviere AH; Hatzikirou H; Lowengrub JS; Frieboes HB; Thompson AM; Cristini V, Mathematical Oncology: How Are the Mathematical and Physical Sciences Contributing to the War on Breast Cancer? Current breast cancer reports, 2010, 2, (3), 121–129. [PubMed: 21151486]

[26]. Cristini V; Frieboes HB; Gatenby R; Caserta S; Ferrari M; Sinek J, Morphologic instability and cancer invasion. Clinical Cancer Research, 2005, 11, (19), 6772–6779. [PubMed: 16203763]

[27]. Cristini V; Lowengrub J Multiscale modeling of cancer: an integrated experimental and mathematical modeling approach. Cambridge University Press, 2010.

[28]. Das H; Wang Z; Niazi MKK; Aggarwal R; Lu J; Kanji S; Das M; Joseph M; Gurcan M; Cristini V, Impact of Diffusion Barriers to Small Cytotoxic Molecules on the Efficacy of Immunotherapy in Breast Cancer. PloS one, 2013, 8, (4), e61398. [PubMed: 23620747]

[29]. Deisboeck TS; Wang Z; Macklin P; Cristini V, Multiscale Cancer Modeling. Annual Review of Biomedical Engineering, 2011, 13, (1), 127–155.

[30]. Edgerton ME; Chuang Y-L; Macklin P; Yang W; Bearer EL; Cristini V, A novel, patient-specific mathematical pathology approach for assessment of surgical volume: application to ductal carcinoma in situ of the breast. Analytical Cellular Pathology, 2011, 34, (5), 247–263.

[31]. Lowengrub JS; Frieboes HB; Jin F; Chuang YL; Li X; Macklin P; Wise SM; Cristini V, Nonlinear modelling of cancer: bridging the gap between cells and tumours. Nonlinearity, 2010, 23, (1), R1. [PubMed: 20808719]

[32]. Macklin P; McDougall S; Anderson ARA; Chaplain MAJ; Cristini V; Lowengrub J, Multiscale modelling and nonlinear simulation of vascular tumour growth. Journal of mathematical biology, 2009, 58, (4), 765–798. [PubMed: 18781303]

[33]. Sanga S; Sinek JP; Frieboes HB; Ferrari M; Fruehauf JP; Cristini V, Mathematical modeling of cancer progression and response to chemotherapy. 2006.

[34]. Wang Z; Butner JD; Kerketta R; Cristini V; Deisboeck TS In Seminars in cancer biology; Elsevier, 2015; Vol. 30, pp 70–78. [PubMed: 24793698]

[35]. Wang Z; Kerketta R; Chuang Y-L; Dogra P; Butner JD; Brocato TA; Day A; Xu R; Shen H; Simbawa E, Theory and experimental validation of a spatio-temporal model of chemotherapy transport to enhance tumor cell kill. PLoS computational biology, 2016, 12, (6), e1004969. [PubMed: 27286441]

[36]. Frieboes HB; Smith BR; Wang Z; Kotsuma M; Ito K; Day A; Cahill B; Flinders C; Mumenthaler SM; Mallick P, Predictive modeling of drug response in non-hodgkin's lymphoma. PloS one, 2015, 10, (6), e0129433. [PubMed: 26061425]

[37]. Wang Z; Deisboeck TS, Mathematical modeling in cancer drug discovery. Drug discovery today, 2013.

[38]. Pascal J; Ashley CE; Wang Z; Brocato TA; Butner JD; Carnes EC; Koay EJ; Brinker CJ; Cristini V, Mechanistic Modeling Identifies Drug-Uptake History as Predictor of Tumor Drug Resistance and Nano-Carrier-Mediated Response. ACS Nano, 2013.

[39]. Wang Z; Butner JD; Cristini V; Deisboeck TS, Integrated PK-PD and agent-based modeling in oncology. Journal of pharmacokinetics and pharmacodynamics, 2015, 42, (2), 179–189. [PubMed: 25588379]

[40]. Wang Z; Deisboeck TS, Dynamic Targeting in Cancer Treatment. Frontiers in physiology, 2019, 10, 96–96. [PubMed: 30890944]

[41]. Brocato TA; Brown-Glaberman U; Wang Z; Selwyn RG; Wilson CM; Wyckoff EF; Lomo LC; Saline JL; Hooda-Nehra A; Pasqualini R, Predicting breast cancer response to neoadjuvant chemotherapy based on tumor vascular features in needle biopsies. JCI insight, 2019.

[42]. Brocato T; Dogra P; Koay EJ; Day A; Chuang Y-L; Wang Z; Cristini V, Understanding Drug Resistance in Breast Cancer with Mathematical Oncology. Current Breast Cancer Reports, 2014, 1–11.

[43]. Pascal J; Bearer EL; Wang Z; Koay EJ; Curley SA; Cristini V, Mechanistic patient-specific predictive correlation of tumor drug response with microenvironment and perfusion measurements. Proceedings of the National Academy of Sciences, 2013, 110, (35), 14266–14271.

[44]. Cristini V; Koay E; Wang Z An Introduction to Physical Oncology: How Mechanistic Mathematical Modeling Can Improve Cancer Therapy Outcomes. CRC Press, 2017.

[45]. Lee JJ; Huang J; England CG; McNally LR; Frieboes HB, Predictive modeling of in vivo response to gemcitabine in pancreatic cancer. PLoS Comput Biol, 2013, 9, (9), e1003231. [PubMed: 24068909]

[46]. Cristini V; Lowengrub J; Nie Q, Nonlinear simulation of tumor growth. Journal of mathematical biology, 2003, 46, (3), 191–224. [PubMed: 12728333]

[47]. Frieboes HB; Jin F; Chuang Y-L; Wise SM; Lowengrub JS; Cristini V, Three-dimensional multispecies nonlinear tumor growth—II: tumor invasion and angiogenesis. Journal of theoretical biology, 2010, 264, (4), 1254–1278. [PubMed: 20303982]

[48]. Li X; Cristini V; Nie Q; Lowengrub JS, Nonlinear three-dimensional simulation of solid tumor growth. DISCRETE AND CONTINUOUS DYNAMICAL SYSTEMS SERIES B, 2007, 7, (3), 581.

[49]. Haeno H; Gonen M; Davis MB; Herman JM; Iacobuzio-Donahue CA; Michor F, Computational modeling of pancreatic cancer reveals kinetics of metastasis suggesting optimum treatment strategies. Cell, 2012, 148, (1–2), 362–375. [PubMed: 22265421]

[50]. Haeno H; Iwasa Y; Michor F, The evolution of two mutations during clonal expansion. Genetics, 2007, 177, (4), 2209–2221. [PubMed: 18073428]

[51]. Yamamoto KN; Nakamura A; Haeno H, The evolution of tumor metastasis during clonal expansion with alterations in metastasis driver genes. Scientific reports, 2015, 5, 15886–15886. [PubMed: 26515895]

[52]. Yamamoto KN; Yachida S; Nakamura A; Niida A; Oshima M; De S; Rosati LM; Herman JM; Iacobuzio-Donahue CA; Haeno H, Personalized Management of Pancreatic Ductal Adenocarcinoma Patients through Computational Modeling. Cancer Res, 2017, 77, (12), 3325–3335. [PubMed: 28381541]

[53]. Yamamoto KN; Nakamura A; Liu LL; Stein S; Tramontano AC; Kartoun U; Shimizu T; Inoue Y; Asakuma M; Haeno H; Kong CY; Uchiyama K; Gonen M; Hur C; Michor F, Computational modeling of pancreatic cancer patients receiving FOLFIRINOX and gemcitabine-based therapies identifies optimum intervention strategies. PLoS One, 2019, 14, (4), e0215409. [PubMed: 31026288]

[54]. Yachida S; Jones S; Bozic I; Antal T; Leary R; Fu B; Kamiyama M; Hruban RH; Eshleman JR; Nowak MA; Velculescu VE; Kinzler KW; Vogelstein B; Iacobuzio-Donahue CA, Distant metastasis occurs late during the genetic evolution of pancreatic cancer. Nature, 2010, 467, (7319), 1114–1117. [PubMed: 20981102]

[55]. Tuckwell HC; Springer Berlin Heidelberg: Berlin, Heidelberg, 1981, pp 162–171.

[56]. Makohon-Moore AP; Matsukuma K; Zhang M; Reiter JG; Gerold JM; Jiao Y; Sikkema L; Attiyeh MA; Yachida S; Sandone C; Hruban RH; Klimstra DS; Papadopoulos N; Nowak MA; Kinzler KW; Vogelstein B; Iacobuzio-Donahue CA, Precancerous neoplastic cells can move through the pancreatic ductal system. Nature, 2018, 561, (7722), 201–205. [PubMed: 30177826]

[57]. Lange F; Rateitschak K; Fitzner B; Pohland R; Wolkenhauer O; Jaster R, Studies on mechanisms of interferon-gamma action in pancreatic cancer using a data-driven and model-based approach. Molecular cancer, 2011, 10, (1), 13. [PubMed: 21310022]

[58]. Lange F; Rateitschak K; Kossow C; Wolkenhauer O; Jaster R, Insights into erlotinib action in pancreatic cancer cells using a combined experimental and mathematical approach. World J Gastroenterol, 2012, 18, (43), 6226–6234. [PubMed: 23180942]

[59]. Louzoun Y; Xue C; Lesinski GB; Friedman A, A mathematical model for pancreatic cancer growth and treatments. J Theor Biol, 2014, 351, 74–82. [PubMed: 24594371]

[60]. Chen J; Weihs D; Vermolen FJ, Computational modeling of therapy on pancreatic cancer in its early stages. Biomechanics and modeling in mechanobiology, 2019.

[61]. Roy M; Finley SD, Computational Model Predicts the Effects of Targeting Cellular Metabolism in Pancreatic Cancer. Frontiers in physiology, 2017, 8, 217. [PubMed: 28446878]

[62]. Gong H; Zuliani P; Wang Q; Clarke EM In 2011 50th IEEE Conference on Decision and Control and European Control Conference, 2011, pp 4855–4860.

[63]. Koay EJ; Lee Y; Cristini V; Lowengrub JS; Kang Y; Lucas FAS; Hobbs BP; Ye R; Elganainy D; Almahariq M; Amer AM; Chatterjee D; Yan H; Park PC; Rios Perez MV; Li D; Garg N; Reiss KA; Yu S; Chauhan A; Zaid M; Nikzad N; Wolff RA; Javle M; Varadhachary GR; Shroff RT; Das P; Lee JE; Ferrari M; Maitra A; Taniguchi CM; Kim MP; Crane CH; Katz MH; Wang H; Bhosale P; Tamm EP; Fleming JB, A Visually Apparent and Quantifiable CT Imaging Feature Identifies Biophysical Subtypes of Pancreatic Ductal Adenocarcinoma. Clinical cancer research : an official journal of the American Association for Cancer Research, 2018, 24, (23), 5883–5894. [PubMed: 30082477]

[64]. Bali MA; Metens T; Denolin V; Delhaye M; Demetter P; Closset J; Matos C, Tumoral and nontumoral pancreas: correlation between quantitative dynamic contrast-enhanced MR imaging and histopathologic parameters. Radiology, 2011, 261, (2), 456–466. [PubMed: 21852570]

[65]. Liu K; Xie P; Peng W; Zhou Z, Dynamic contrast-enhanced magnetic resonance imaging for pancreatic ductal adenocarcinoma at 3.0-T magnetic resonance: correlation with histopathology. J Comput Assist Tomogr, 2015, 39, (1), 13–18. [PubMed: 25340589]

[66]. Root A, Mathematical Modeling of The Challenge to Detect Pancreatic Adenocarcinoma Early with Biomarkers. Challenges, 2019, 10, (1), 26.

[67]. Koay EJ; Truty MJ; Cristini V; Thomas RM; Chen R; Chatterjee D; Kang Y; Bhosale PR; Tamm EP; Crane CH; Javle M; Katz MH; Gottumukkala VN; Rozner MA; Shen H; Lee JE; Wang H; Chen Y; Plunkett W; Abbruzzese JL; Wolff RA; Varadhachary GR; Ferrari M; Fleming JB, Transport properties of pancreatic cancer describe gemcitabine delivery and response. J Clin Invest, 2014, 124, (4), 1525–1536. [PubMed: 24614108]

[68]. Koay EJ; Baio FE; Ondari A; Truty MJ; Cristini V; Thomas RM; Chen R; Chatterjee D; Kang Y; Zhang J; Court L; Bhosale PR; Tamm EP; Qayyum A; Crane CH; Javle M; Katz MH; Gottumukkala VN; Rozner MA; Shen H; Lee JE; Wang H; Chen Y; Plunkett W; Abbruzzese JL; Wolff RA; Maitra A; Ferrari M; Varadhachary GR; Fleming JB, Intra-tumoral heterogeneity of gemcitabine delivery and mass transport in human pancreatic cancer. Phys Biol, 2014, 11, (6), 065002. [PubMed: 25427073]

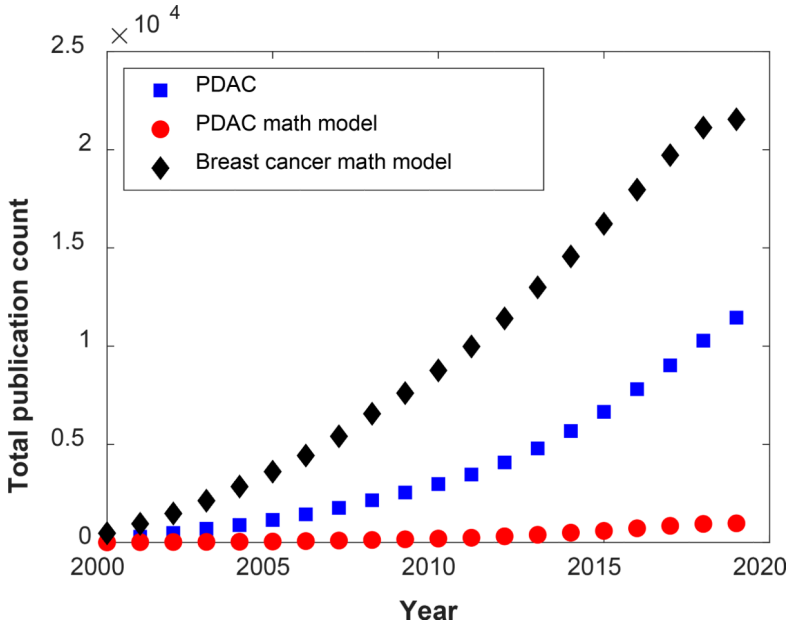


**Figure 1.**

Graph showing PubMed results of total publication count over the last two decades (1/1/2000–9/28/2019) for the keywords ‘pancreatic ductal adenocarcinoma’ (square shapes), ‘pancreatic ductal adenocarcinoma mathematical modeling’ (circle shapes), and ‘breast cancer mathematical modeling’ (diamond shapes).

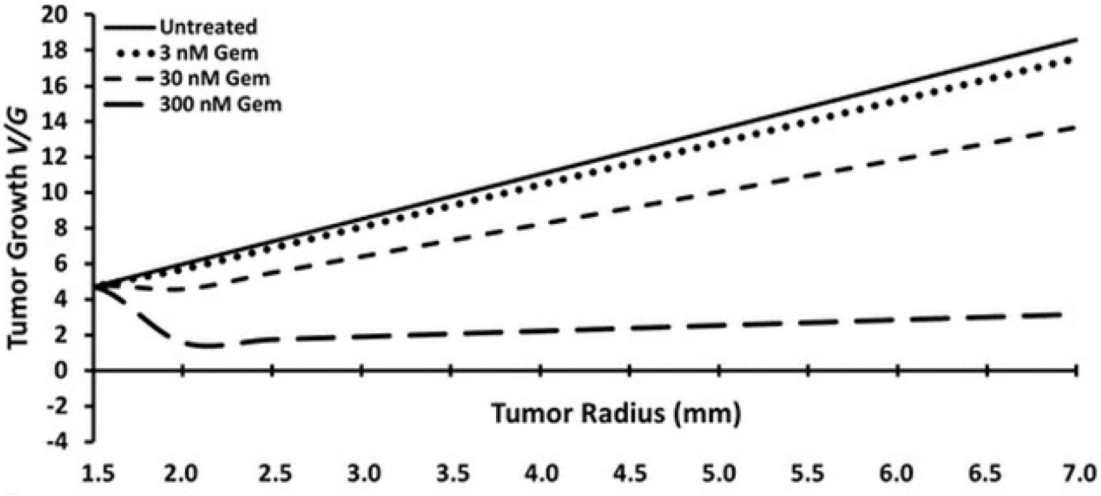


**Figure 2.**

Progression of tumor growth ( $V/G$) and tumor radius as a function of the concentration of gemcitabine predicted by the model. Reproduced with permission from Lee *et al.* [45].

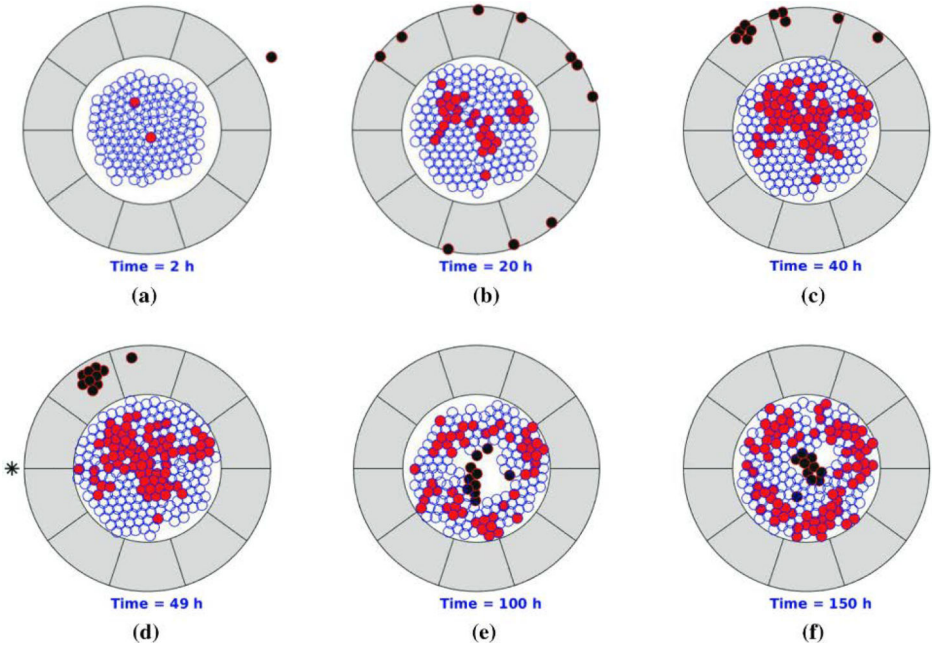


**Figure 3.**

Schematic of model domain showing epithelial cells, cancer cells, T-lymphocytes, and extracellular matrix in blue, red, black, and gray colors, respectively. Black asterisk represents the site of drug injection. Reproduced with permission from Chen *et al.* [60].

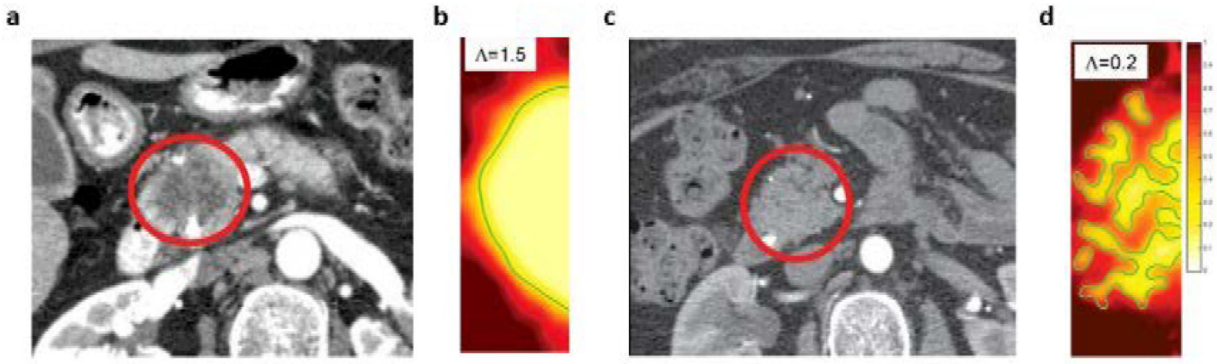


**Figure 4.**

**a,c)** Tumor images from CT scans (circled in red) showing high-delta (**a**) and low-delta (**c**) tumors, and **b,d)** corresponding simulations of the mathematical model showing distinct tumor-healthy tissue interface patterns that explain the CT scan observations. Values of the stability parameter Λ used for simulations are shown in the inset. Reproduced with permission from Koay *et al.* [63].

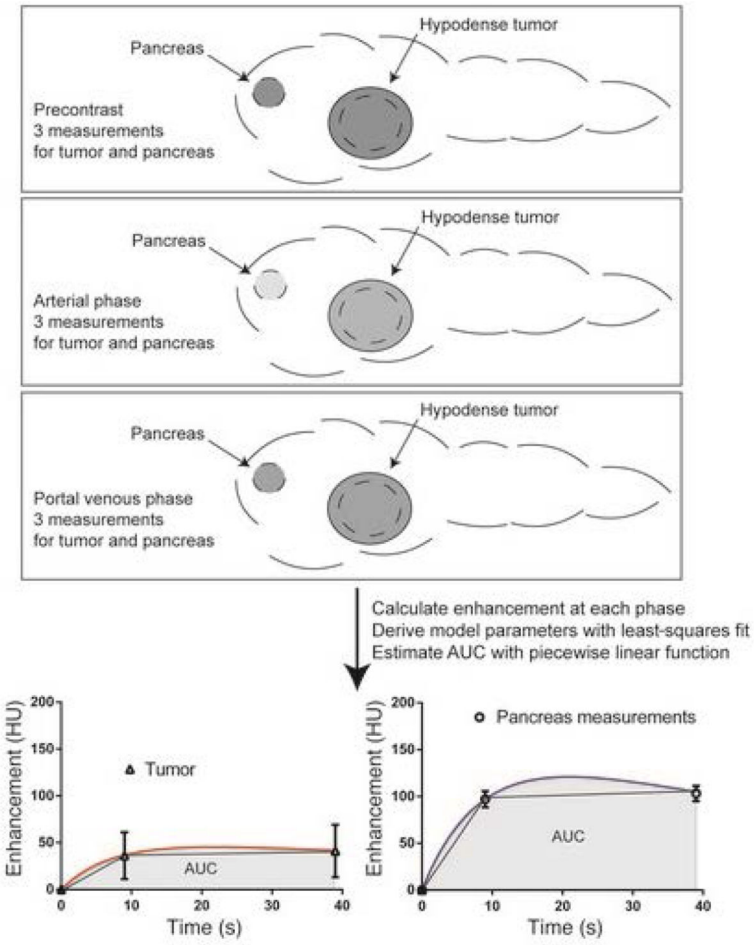


**Figure 5.**

A schematic showing the protocol for measurement of transport properties through CT imaging. Abdominal CT scans at the precontrast, arterial phase, and portal venous phase are obtained to acquire the contrast enhancement kinetics in the tumor and healthy pancreatic regions. The mathematical model is then fit to the imaging data to obtain an estimate for the area under the curve for both tumor and healthy regions. Reproduced with permission from Koay *et al.* [67].